Title:

Chloride ions evoke taste sensations by binding to the extracellular ligand-binding domain of sweet/umami taste receptors

Authors:

Nanako Atsumi[1†], Keiko Yasumatsu[2†], Yuriko Takashina[3], Chiaki Ito[1], Norihisa Yasui[1], Robert F. Margolskee[4], Atsuko Yamashita[1]

[†]These authors contributed equally to this work.

Affiliation:

[1]Graduate School of Medicine, Dentistry and Pharmaceutical Sciences, Okayama University, Okayama, Japan, [2]Oral Health Science Center, Tokyo Dental College, Tokyo, [3]School of Pharmaceutical Sciences, Okayama University, Okayama, Japan, [4]Monell Chemical Senses Center, Philadelphia, PA, USA.

Corresponding author:

Atsuko Yamashita, Graduate School of Medicine, Dentistry and Pharmaceutical Sciences, Okayama University, 1-1-1, Tsushima-naka, Kita-ku, Okayama 600-8530, Japan. Fax: +81-86-251-7974. E-mail: a_yama@okayama-u.ac.jp.

Abstract

Salt taste sensation is multifaceted: NaCl at low or high concentrations is preferably or aversively perceived through distinct pathways. Cl^- is thought to participate in taste sensation through an unknown mechanism. Here we describe Cl^- ion binding and the response of taste receptor type 1 (T1r), a receptor family composing sweet/umami receptors. The T1r2a/T1r3 heterodimer from the medaka fish, currently the sole T1r amenable to structural analyses, exhibited a specific Cl^- binding in the vicinity of the amino-acid-binding site in the ligand-binding domain (LBD) of T1r3, which is likely conserved across species, including human T1r3. The Cl^- binding induced a conformational change in T1r2a/T1r3LBD at sub- to low-mM concentrations similar to canonical taste substances. Furthermore, oral Cl^- application to mice increased impulse frequencies of taste nerves connected to T1r-expressing taste cells and promoted their behavioral preferences attenuated by a T1r-specific blocker or T1r3 knock-out. These results suggest that the Cl^- evokes taste sensations by binding to T1r, thereby serving as another preferred salt taste pathway at a low concentration.

Introduction

The taste sensation is initiated by specific interactions between chemicals in food and taste receptors in taste buds in the oral cavity. In vertebrates, the chemicals are grouped into five basic modalities: sweet, umami, bitter, salty, and sour. This sensation occurs through taste receptor recognition specific to a group of chemicals representing each taste modality (Taruno *et al*, 2021). Regarding the salty taste, the preferable taste, ~100 mM concentration of table salt, is evoked by specific interaction between the epithelial sodium channel (ENaC) and sodium ion (Chandrashekar *et al*, 2010) (Figure 1). Notably, salt sensation exhibits multifaced properties (Roper, 2015), thereby suggesting the existence of an adequate concentration range for salt intake to maintain the homeostasis of body fluid concentration. For example, high concentrations of salt over levels perceived as a preferred taste, such as ~500 mM, stimulate bitter and sour taste cells and are perceived as an aversive taste (Oka *et al*, 2013). Conversely, low salt concentrations under the "preferable" concentration, such as several mM to a hundred mM concentrations, are perceived as sweet by human panels (Bartoshuk *et al*, 1964; Bartoshuk *et al*, 1978; Cardello, 1979). However, its mechanism has never been extensively pursued. The various impacts of the salt taste sensation indicate multiple salt detection pathways in taste buds (Roper, 2015). Moreover, another component of table salt, the chloride ion, participates in taste sensation because of the existence of the "anion effect": the salty taste is most strongly perceived when the counter anion is a chloride ion (Ye *et al*, 1991). Several reports suggested a certain cellular/molecular machinery underlying anion-sensitive Na^+-detection or Cl^--detection, which is independent of ENaC (Lewandowski *et al*, 2016; Roebber *et al*, 2019). Indeed, a recent study indicated that transmembrane channel-like 4 (TMC4) expressed in taste buds involves high-concentration Cl^--sensation (Kasahara *et al*, 2021). Nevertheless, no candidate molecule capable of sensing low or preferable concentrations of Cl^- has been elucidated. Therefore, the complete understanding of salt taste

61 sensation, including the mechanism of chloride ion detection, remains unclear.

62 Unlike salt taste sensation, those for nutrients as sugars, amino acids, and
63 nucleotides are understood as sweet and umami sensations through specific receptor proteins
64 (Li *et al*, 2002; Nelson *et al*, 2002; Nelson *et al*, 2001). Sweet and umami receptors are
65 composed of taste receptor type 1 (T1r) proteins in the class C G protein-coupled receptor
66 family. In humans, the T1r1/T1r3 heterodimer serves as the umami taste receptor and
67 responds to amino acids as L-glutamate and aspartate, and nucleotides. In contrast, the
68 T1r2/T1r3 heterodimer is the sweet taste receptor and responds to sugars. We previously
69 elucidated the crystallographic structure of the medaka fish T1r2a/T1r3 extracellular
70 ligand-binding domain (LBD) (Nuemket *et al*, 2017), which is currently the sole reported
71 structure of T1rs. In the structure, the amino acid-binding was observed in the middle of the
72 LBD of T1r2a and T1r3 subunits, which was consistent with the fact that T1r2a/T1r3 is an
73 amino-acid receptor (Oike *et al*, 2007). Furthermore, chloride ion binding was found in the
74 vicinity of the amino-acid binding site in T1r3 (Figure 2A). So far, the physiological
75 significance of Cl^--binding for T1rs functions remains unexplored. Nevertheless, chloride
76 ions regulate other receptors in class C G protein-coupled receptors (GPCRs), such as
77 metabotropic glutamate receptors (mGluRs) and calcium-sensing receptors (CaSRs), and act
78 as positive modulators for agonist binding (Eriksen & Thomsen, 1995; Kuang & Hampson,
79 2006; Liu *et al*, 2020; Tora *et al*, 2018; Tora *et al*, 2015). The potential effect of Cl^--binding
80 on T1r receptor function is of significant interest under these conditions.

81 Here, we investigated the Cl^- actions on T1rs using structural, biophysical, and
82 physiological analyses. The Cl^- binding to the LBD was investigated using the medaka fish
83 T1r2a/T1r3LBD, which is amenable to structural and biophysical analyses. Since the Cl^-
84 -binding site in T1r3 was conserved across various species, taste nerve recordings from mice
85 were used to investigate the physiological significance of Cl^-. The results suggest that Cl^-

86 induces the moderate response via T1rs, thereby implying that T1rs are involved in Cl^-
87 sensation in taste buds.
88
89 **Results**
90 **Cl^--binding site in T1r3**
91 In the previously reported structure of T1r2a/T1r3LBD crystallized in the presence of NaCl,
92 bound Cl^- was identified based on electron density and binding distances (Nuemket *et al.*,
93 2017). To verify the Cl^--binding, Cl^- in the T1r2a/T1r3LBD crystal was substituted with Br^-,
94 a halogen ion amenable for specific detection by anomalous scattering using a synchrotron
95 light source (Figure 2−figure supplement 1). The diffraction data from the crystal resulted in
96 an anomalous difference Fourier peak at 14.1 σ at the site in the vicinity of the amino-acid
97 binding site in T1r3, where Cl^- was originally bound (Figure 2B, Figure 2—figure
98 supplement 2). For further confirmation, the anomalous data of the original crystal containing
99 Cl^- was collected at 2.7 Å, where the anomalous peak for Cl and several other elements such
100 as Ca or S can be detected (Figure 2—figure supplement 1). The resultant anomalous
101 difference Fourier map showed a peak at the bound Cl^- position, while all the other peaks
102 were observed at the S atoms in the protein (Figure 2C, Figure 2—figure supplement 2).
103 These results verify that the site is able to bind halogen ions, likely accommodating Cl^- under
104 physiological conditions.
105 Cl^- was coordinated at the binding site by the side-chain hydroxyl group of Thr105
106 and the main-chain amide groups of Gln148 and Ser149 (Figure 2D). These main-chain
107 coordinating residues are followed by Ser150, a critical residue for binding amino-acid
108 ligands (Nuemket *et al.*, 2017). Furthermore, the loop regions where Thr105 and the
109 Gln148-Ser150 locate are followed by helices B and C, respectively. These helices are
110 essential structural units at the heterodimer interface (Nuemket *et al.*, 2017) (Figure 2A).

111 They are known to reorient upon agonist binding, resulting in conformation rearrangement of
112 the subunits in the dimer, likely inducing receptor activation in class C GPCRs (Koehl *et al*,
113 2019; Kunishima *et al*, 2000). In addition, the side-chain hydroxyl group of Ser149, which
114 serves as a cap for the positive helix dipole of helix C, simultaneously functions as a distal
115 ligand for Cl^- coordination. Therefore, the Cl^- binding at this site is important for organizing
116 the structure of the amino-acid binding site and the heterodimer interface.

117 The Cl^--binding site observed in the crystal structure is most likely conserved
118 among T1r3s in various organisms, such as humans (Figure 2E). Thr105, the residue that
119 provides the side-chain-coordinating ligand for Cl^--binding, is strictly conserved as either
120 serine or threonine among T1r3s. Additionally, the amino-acid sequence motifs surrounding
121 the main-chain-coordinating ligands, $FP^{45}L$ and $VIGP\zeta^{148}\zeta^{149}$, where "ζ" is a hydrophilic
122 amino acid, are well conserved to present the main-chain amide groups to coordinate Cl^- with
123 an appropriate geometry. Notably, the site structurally corresponds to the Cl^--binding site in
124 the hormone-binding domain of the atrial natriuretic peptide receptor (ANPR) (Figure 2F, 2G),
125 in which Cl^- positively regulates the peptide hormone binding (Misono, 2000). Although
126 ANPR is not a member of class C GPCR, the hormone-binding domain in ANPR shares a
127 similar structural fold with LBD of T1rs and other class C GPCRs, and bacterial
128 periplasmic-binding proteins (Kunishima *et al.*, 2000; van den Akker *et al*, 2000).
129 Accordingly, the conservation of the structure and the sequence motif at the Cl^--binding site
130 at ANPR is also observed on mGluRs (Ogawa *et al*, 2010). Indeed, Cl^- binding at the site
131 corresponding to that in T1r3 was observed in several mGluR and CaSR structures (Monn *et*
132 *al*, 2015b; Zhang *et al*, 2016) (Figure 2F, 2G) and was identified as a potential site responsible
133 for regulating agonist binding (Liu *et al.*, 2020; Tora *et al.*, 2015). These results strongly
134 imply the possibility that Cl^- has some actions on T1r receptor functions.

135 In contrast, conservation at the Thr105 position was not observed among T1r1 and

T1r2 (Figure 2E). Evidently, no significant anomalous peak derived from Br^-- or Cl^--binding was observed in the crystal structure at the corresponding site in T1r2a (Figure 2B, 2C). His100 in T1r2a, which corresponds to Thr105 in T1r3, adopted a significantly different side-chain conformation from that of Thr105 in T1r3 (Figure 2—figure supplement 2). Therefore, T1r1 and T1r2's ability to bind Cl^- is unlikely.

In addition to the Cl^--binding site discussed above, the Br^--substituted crystal exhibited an anomalous peak at 8.5 σ in T1r2a, at a position close to the Lys265 side-chain ε-amino group (Figure 2B, Figure 2—figure supplement 2). Nevertheless, Cl^--binding was not observed in the original Cl^--contained crystal. This is further confirmed by the absence of an anomalous peak at this position in the data collected at 2.7 Å (Figure 2C, Figure 2—figure supplement 2). Therefore, the site might have the ability to bind anions such as Br^- or larger; but be not specific to Cl^-. In human T1r1, the residue corresponding to Lys265 (Arg277) was suggested as a critical residue for activities of inosine monophosphate, an umami enhancer (Zhang *et al*, 2008).

Cl^--binding properties in T1r2a/T1r3LBD

To investigate the Cl^- actions on T1r functions, we first examined the properties of the Cl^--binding to medaka T1r2a/T1r3LBD using various biophysical techniques. For this purpose, the purified T1r2a/T1r3LBD was subjected to differential scanning fluorimetry (DSF), which we previously used for the amino acid-binding analysis (Yoshida *et al*, 2019). In order to prepare a Cl^--free condition, Cl^- in the sample was substituted with gluconate, as it is unlikely accommodated in the Cl^--site due to its much larger size. We confirmed that gluconate does not serve as a ligand for T1r2a/T1r3LBD (Figure 3—figure supplement 1).

The addition of Cl^- to the Cl^--free T1r2a/T1r3LBD sample resulted in thermal stabilization of the protein (Figure 3A), which is indicative of Cl^- binding to the protein. The

apparent K_d value for Cl^- estimated by the melting temperatures (T_m) at various Cl^- concentrations was ~110 μM (Figure 3B, Table 1). The Cl^--dependent thermal stabilization was confirmed by the fluorescence-detection size-exclusion chromatography-based thermostability (FSEC-TS) assay (Hattori *et al*, 2012) (Figure 3C, Table 1). However, the Cl^--dependent stabilization was not observed on T1r2a/T1r3 with the Cl^--site mutation, T105A in T1r3. In the case of this mutant, the T_m values for both in the presence and absence of Cl^- was similar to the values obtained for the wild-type protein in the absence of Cl^- (Figure 3C, Figure 3—figure supplement 1, Table 1). These results indicate that the Cl^- effect attributed to the identical site where the Cl^--binding was observed in the crystal structure of T1r3.

Next, we examined the consequence of the Cl^--binding to T1r2a/T1r3LBD via Förster resonance energy transfer (FRET) using the fluorescent protein-fused sample. Class C GPCRs commonly exhibit agonist-induced conformational changes in LBD, such as the dimer rearrangement, which is essential for receptor activation and signaling (Ellaithy *et al*, 2020; Koehl *et al.*, 2019; Kunishima *et al.*, 2000; Lin *et al*, 2021). Consistent with this, we previously reported that T1r2a/T1r3LBD shows conformational change concomitant with the binding of amino acids, which can be detected as increased FRET intensity (Nango *et al*, 2016). Notably, adding Cl^- to the fluorescent protein-fused T1r2a/T1r3LBD also increased FRET intensities, similar to amino acids (Figure 3D). The EC_{50} for Cl^--induced FRET signal change was determined as ~1 mM (Table 1). Note that both DSF and FRET estimations have some degree of error: the former produced slightly lower values than the latter, particularly in the case of weak affinities in the mM concentration range (Yoshida *et al.*, 2019). As such, although the EC_{50} value determined by FRET was slightly higher than the apparent K_d value of Cl^- determined by DSF, the two are most likely relevant. Considering that the Cl^--binding site is located adjacent to the dimer interface, which exhibits reorientation upon agonist binding (Figure 2D), the results suggest that the Cl^-binding to T1r2a/T1r3LBD induces a

conformational rearrangement of T1r2a/T1r3LBD similar to its agonist amino acid. Nevertheless, the extent of the FRET change induced by Cl^- was smaller than the changes induced by amino acids, such as ~1/2 of the latter (Figure 3E). Therefore, the results suggest that the extent of the conformational change induced by Cl^- is smaller than the change induced by amino acids. The extent of Cl^--dependent FRET index change was reduced on T1r2a/T1r3 with the Cl^--site mutation, T105A in T1r3 (Figure 3E). Considering that the amino-acid-dependent change in the mutant was also significantly reduced (Figure 3E), the T105A mutation on T1r3 might result in losing the ability of the conformational change induced by Cl^-- and amino-acid bindings, although the possibility of deactivation of the protein during preparation due to its low stability cannot be excluded.

In addition to the Cl^--binding effect, the Cl^- effect on amino-acid binding to T1r2a/T1r3LBD was investigated by FRET and isothermal calorimetry (ITC). The K_d values for L-glutamine binding determined by ITC, as well as the EC_{50} values and the other parameters for L-glutamine-induced conformational change determined by FRET, did not differ in the presence and absence of Cl^- (Figure 3F, Figure 3—figure supplement 1, and Table 1). These results indicated that the Cl^- binding had no significant effect on the binding of L-glutamine, a representative taste substance, at least for T1r2a/T1r3LBD from medaka fish.

Taste response to Cl^- through T1rs in mouse

Biophysical studies on T1r2a/T1r3LBD from medaka fish suggested that Cl^-binding to T1r3LBD induces a conformational change similar to that of an agonist without affecting agonist binding. As described above, the Cl^--binding site is likely conserved among T1r3 in various species, such as those in mammals. Therefore, we analyzed single fiber responses from mouse chorda tympani nerve to investigate the physiological effect of Cl^- on taste

211 sensation. While conventional cell-based receptor assay systems are affected by changes in
212 extracellular ionic components, the application of various solutions to the taste pore side of
213 the taste buds projected to taste nerve systems, are transduced exclusively as “taste” signals,
214 without inducing the other cellular responses derived from the ionic component changes in
215 the surrounding environment.

216 We first identified nerve fibers that connect to T1r-expressing taste cells in
217 wild-type (WT) mice, i.e., that receive taste information from cells likely possessing sweet
218 (T1r2/T1r3) and umami (T1r1/T1r3) receptors (Yasumatsu *et al*, 2012). The identification was
219 evidenced by responses to T1r agonists, such as sugars and amino acids, which were inhibited
220 by gurmarin (Gur), a T1r-specific blocker (Daly *et al*, 2013; Margolskee *et al*, 2007;
221 Ninomiya & Imoto, 1995; Ninomiya *et al*, 1999). Then, we examined the responses to Cl^- in
222 these fibers. Remarkably, the fibers also exhibited responses induced by Cl^-, which was
223 applied as a form of NMDG-Cl devoid of the known salty taste stimulant, sodium ion (Figure
224 4A). Cl^--induced impulse frequencies from the nerves increased in a concentration-dependent
225 manner (Figure 4B). The responses to NMDG-Cl, NaCl, and KCl at the same concentrations
226 did not differ significantly (repeated measures analysis of variance [ANOVA], $P > 0.05$),
227 whereas responses to NMDG-gluconate were significantly smaller than those to NMDG-Cl
228 (repeated measures ANOVA: $F_{(1, 43)} = 31.33$, $P < 0.001$) and did not induce explicit responses
229 up to 10 mM. These results confirmed that the observed responses were attributed to Cl^-. All
230 responses to Cl^-, regardless of the type of counter cations, were significantly decreased by
231 lingual treatment with Gur (Figure 4B, repeated measures ANOVA: $F_{(1, 42)} = 56.65$, $P < 0.001$
232 for NMDG-Cl; $F_{(1, 50)} = 24.78$, $P < 0.001$ for NaCl; and $F_{(1, 45)} = 35.72$, $P < 0.001$ for KCl).
233 Furthermore, responses to Cl^- in T1r3-KO mice were significantly lower than those in WT
234 mice (repeated measures ANOVA: $F_{(1, 43)} = 25.36$, $P < 0.001$; Figure 4C). The results indicate
235 that the observed Cl^--dependent responses were mediated by T1r. Notably, the Cl^-

-concentration range that induced nerve responses was lower (≤ ~10 mM) than that for Na^+-detection by ENaC when applied as the NaCl form (≥ ~30 mM) (Chandrashekar *et al.*, 2010) but is consistent with those for Cl^--binding and Cl^--induced conformational change observed on T1r2a/T1r3LBD (Table 1). These results suggest that a low Cl^- concentration is sensorily detected via T1r in taste buds. Although the responses induced by known taste substances for T1rs, such as sugars and amino acids, range from tens to hundreds of impulse frequencies per 10 s (Yasumatsu *et al.*, 2012); the maximum response level induced by Cl^- was low, ~10 per 10 s (Figure 4B). According to our observations, Cl^- likely produces a "light" taste sensation compared with other known taste substances.

Next, to examine the physiological interaction between a canonical taste substance for mouse T1r and Cl^-, we recorded responses to 20 mM L-glutamine or 100 mM sucrose from T1r1/T1r3- and T1r2/T1r3-expressing cells, respectively, with or without NMDG-Cl from the same T1r-connecting single fibers (Figure 4A). The concentrations for the taste substances were set to induce responses greater than the baseline but less than maximum. As shown in Figure 4D, the response to L-glutamine or sucrose increased significantly by adding 10 mM NMDG-Cl (paired *t*-test, $t2 = 7.56$, $p = 0.017$ for L-glutamine and $t2 = 5.05$, $p = 0.037$ for sucrose). We confirmed that these responses had been suppressed by a lingual treatment of Gur in the presence ($t2 = 6.73$, $p = 0.021$ for L-glutamine and $t2 = 8.80$, $p = 0.013$ for sucrose) or absence ($t2 = 8.32$, $p = 0.014$ for L-glutamine and $t2 = 11.72$, $p = 0.007$ for sucrose) of NMDG-Cl to a similar extent and a similar level to the responses in T1r3-KO mice. Moreover, the responses to the mixtures did not differ significantly from the summation of the responses to each solution ($t2 = 2.34$, $p = 0.145$ for L-glutamine and $t2 = 2.31$, $p = 0.147$ for sucrose). The results suggest that the simultaneous binding of Cl^- and a canonical taste substance, such as amino acids and sugars, to T1r do not cause synergistic responses.

Finally, we addressed whether T1r-mediated Cl^- responses observed in the taste

nerves involve taste perception. Thus far, most reported behavioral assays for examining the gustatory detection of NaCl were performed with concentrations above ~30 mM, which can induce ENaC-mediated responses. Nevertheless, a few reports have shown that NaCl solution induced higher consumption relative to water even below 10 mM concentration (Dyr *et al*, 2014; Stewart *et al*, 1994), which is below the range inducing ENaC-mediated responses (Chandrashekar *et al.*, 2010) but within what we observed in the Cl^--induced taste nerve responses via T1r. For verification, we performed a mouse two-bottle choice test using NMDG-Cl solution and analyzed the preference relative to water. The mouse preferred water containing 10 mM NMDG-Cl, which was abolished by the application of Gur (Figure 4E, 4F). These results suggest that Cl^- is preferably perceived through taste signal transduction mediated by T1r.

Discussion

In this study, Cl^- is found to specifically interact with the LBD in T1r3, a common component of sweet and umami taste receptors, and induces a conformational change in the receptor's LBD region. The Cl^- binding to T1r in taste cells is likely further transmitted to the sweet taste nervous system, resulting in a light yet preferable taste sensation. Since T1rs are conserved across vertebrates and the Cl^--binding site is likely conserved among T1r3 in various organisms, T1r-mediated Cl^- responses might be common in many animals, such as humans. Evidently, the concentration range for the Cl^--induced conformational change of medaka T1r2a/T1r3LBD and increase in murine sweet nerve impulses observed in this study (i.e., $\leq$ ~10 mM) agrees with the NaCl concentration perceived as "sweet" by humans (Bartoshuk *et al.*, 1964; Bartoshuk *et al.*, 1978; Cardello, 1979) (Figure 1). Additionally, the sweet sensation induced by NaCl was reportedly suppressed by topical application of *Gymnema sylvestre* (Bartoshuk *et al.*, 1978), containing Gymnemic acids, which are specific

286 inhibitors of human sweet taste receptor T1r2/T1r3 (Sanematsu *et al*, 2014). Overall, these
287 results agree with the involvement of T1rs in the Cl^--taste detection. These findings agree
288 with an earlier hypothesis by Bartoshuk and colleagues that dilute NaCl contains a sweet
289 stimulus that interacts with the same receptor molecules as sucrose (Bartoshuk *et al.*, 1978).
290 The reported "sweet" sensation by low NaCl concentration faded out at the concentrations
291 detected as "salty" (Bartoshuk *et al.*, 1964; Bartoshuk *et al.*, 1978; Cardello, 1979), thereby
292 agreeing with the fact that we might be unaware that table salt is sweet at such concentrations.
293 The phenomenon could be explained by "mixture suppression" (Bartoshuk, 1975; Keast &
294 Breslin, 2002; Stevens, 1996), such that a light sweet sensation is masked by an intense salty
295 sensation in a higher concentration range of NaCl.

296 The Cl^- perception at low salt concentrations found in this study is achieved via the
297 T1rs-mediating taste system, which transduces information as a preferred taste by nature.
298 Since Cl^- is also a component of table salt, this system might serve as another pathway for
299 preferred salt perception promoting intake along with the pathway for Na^+ perception as a
300 preferred taste via taste cells that express the Na^+ receptor ENaC and a purinergic
301 neurotransmission channel CALHM1/3 (Nomura *et al*, 2020). In contrast, the T1r-mediated
302 Cl^--sensing observed in this study shows several different properties from those of cells or the
303 molecules reportedly exhibiting anion-sensitive Na^+ detection or Cl^- detection in taste buds
304 thus far. Specifically, the anion-sensitive Na^+-responding taste cells reported by Lewandowski
305 *et al.* are type 3 cells, which include sour- but not sweet-responding cells (Lewandowski *et al.*,
306 2016). The Cl^--detection pathway reported by Roebber *et al.* was observed in type 2 cells,
307 which include both sweet- and bitter-responding cells, but was inhibited by a blocker of
308 phospholipase C, which mediates sweet- and bitter-signaling downstream of T1r and bitter
309 receptors (Roebber *et al.*, 2019). The Cl^--responses mediated by TMC4 were observed in the
310 glossopharyngeal nerve but not in the chorda tympani nerve wherein T1r-mediated responses

were observed (Kasahara *et al.*, 2021). Notably, responses by these reported pathways were tested by much higher concentrations of NaCl, typically in the several hundred mM range (Kasahara *et al.*, 2021; Lewandowski *et al.*, 2016; Roebber *et al.*, 2019), than those used in this study. These results imply that there may be multiple distinct concentration-dependent pathways for Cl^- detection in taste buds. Given that high NaCl concentration is transduced as an aversive taste through bitter and sour taste cells (Oka *et al.*, 2013), the relevance between the reported high Cl^--responsive pathways and high NaCl responses by bitter and sour cells is of interest, as pointed out by the previous studies, and will require further investigation.

Salt taste sensation and natriuresis are critical physiological processes that regulate sodium intake and excretion to maintain body fluid homeostasis. Intriguingly, both processes were found to use the counter anion Cl^- to regulate the molecular functions of the receptors, T1rs and ANPRs, which share a similar extracellular protein architecture with a conserved Cl^--binding site. In the case of ANPR, mGluRs, and CaSR, positive allosteric modulations by Cl^- for agonist binding have been observed, with some variations in the extent of the enhancement (Eriksen & Thomsen, 1995; Kuang & Hampson, 2006; Liu *et al.*, 2020; Tora *et al.*, 2018; Tora *et al.*, 2015). Whether the Cl^- actions on T1rs of other subtypes or from other organisms have some variance is yet to be examined.

Materials and methods

Crystallography

All protein samples used for structural and functional analyses were prepared using Drosophila S2 cells (Invitrogen) or high-expression clones for each protein sample established from S2 cells in previous studies (Nuemket *et al.*, 2017; Yamashita *et al*, 2017). No authentication or test for mycoplasma contamination was performed.

The L-glutamine-bound T1r2a/T1r3LBD crystals, in complex with a crystallization

chaperone Fab16A, were prepared in the presence of NaCl as described (Nuemket *et al.*, 2017). For the preparation of the Br^--substituted crystals, the obtained crystals were soaked in a mother liquor consisting of 100 mM MES-Tris, pH 6.0, 50 mM NaBr, 17% PEG1500, 5% PEG400, 5 mM L-glutamine, 2 mM $CaCl_2$, cryoprotected by gradually increasing the concentration of glycerol to 10%, incubated for 2 hours, and flash-frozen.

The X-ray diffraction data were collected at the SPring-8 beamline BL41XU using a PILATUS6M detector (DECTRIS) at wavelength 0.9194 Å or at the Photon Factory beamline BL-1A using an EIGER X4M detector (DECTRIS) at wavelength 2.7 Å. The data were processed with XDS (Kabsch, 2010) (Figure 2—figure supplement 1). The phases for anomalous difference Fourier map calculation were obtained by molecular replacement methods with the program PHASER (McCoy *et al*, 2007), using the structures of a single unit of the mfT1r2a-3LBD-Fab16A complex (PDB ID: 5X2M; ligands and water models were removed) (Nuemket *et al.*, 2017) as the search model (the R/R_{free} of the model for the Br^--data collected at 0.9194 Å: 0.248/0.350; the Cl^--data collected at 2.7 Å: 0.233/0.339).

Differential scanning fluorimetry (DSF)

Differential scanning fluorimetry was performed as previously described (Yoshida *et al.*, 2019). The purified mfT1R2a/3LBD heterodimer protein was prepared (Nango *et al.*, 2016) and dialyzed with buffer A (20 mM HEPES-NaOH, 300 mM sodium gluconate, pH 7.5) to remove Cl^-. 1 µg of the dialyzed protein sample was mixed with Protein Thermal Shift Dye (Applied Biosystems) and 0.003 – 10 mM NaCl in 20 µL of buffer A. The mixture solutions were then loaded to a MicroAmpR Fast Optical 48-Well Reaction Plate (Applied Biosystems). Fluorescent intensities were measured by the StepOne Real-Time PCR System (Applied Biosystems) while the temperature raised from 25 °C to 99 °C with a velocity of 0.022 °C/sec. For detection, the reporter and quencher were set as “ROX” and “none,” respectively. The

apparent melting transition temperature (T_m) was determined using the maximum of the derivatives of the melt curve (dFluorescence/dT) by Protein Thermal Shift Software version 1.3 (Applied Biosystems). The apparent dissociation constant ($K_{d\text{-}app}$) for Cl^- derived from the T_m values at different NaCl concentrations was estimated using a thermodynamic model proposed by Schellman (Schellman, 1975) as described (Yoshida *et al.*, 2019). The sample sizes for the analyses by DSF, as well as Förster resonance energy transfer and isothermal titration calorimetry described below, were set to obtain reliable values based on the experiences in the previous studies (Nango *et al.*, 2016; Nuemket *et al.*, 2017; Yoshida *et al.*, 2019).

Förster resonance energy transfer (FRET)

FRET analysis was performed as described previously (Nango *et al.*, 2016; Nuemket *et al.*, 2017). The WT T1r2aLBD-Cerulean and T1r3LBD-Venus fusion heterodimer proteins were prepared as described (Nuemket *et al.*, 2017). For the mutant protein preparation, a T1r3-T105A mutation was introduced into the vector pAc-mfT1r3aL-Ve (Nango *et al.*, 2016) using polymerase chain reaction. The mutant expression vector was co-introduced with pAc-mfT1r2aL-Ce (Nango *et al.*, 2016) to Drosophila S2 cells using Polyethyleneimine (PEI) "MAX" (Polysciences) as previously described (Bleckmann *et al*, 2019) with a ratio of 0.5 µg pAc-mfT1r2aL-Ce, 0.5-µg pAc- mfT1r3aL-Ve-T105A, and 10-µg PEI to ~1 × 10^6 cells. Protein expression and purification were conducted similarly as for the WT protein.

For the Cl^--titration, the purified protein samples were dialyzed against buffer A in the presence of 1-mM L-alanine. Afterward, the samples were diluted with buffer A to reduce the remaining L-alanine concentration below 1 µM (< ~1/100 of EC_{50} (Nango *et al.*, 2016; Nuemket *et al.*, 2017)), and then incubated in the presence of 0.001–10 mM NaCl or 1 mM L-glutamine in buffer A at 4°C overnight. For L-glutamine titration in the presence or absence

386 of Cl^-, the protein solution was dialyzed with buffer B (20 mM HEPES-Tris, 300 mM NaCl,
387 pH 7.5) or buffer C (20 mM HEPES-Tris, 300 mM sodium gluconate, pH 7.5) in the presence
388 of 1 mM L-alanine to prepare the conditions with or without Cl^-, respectively. Then, the
389 samples were diluted with buffer B or C to reduce the remaining L-alanine concentration
390 below 1 μM and then incubated in the presence of 0.01–1000 μM L-glutamine at 4°C
391 overnight. Fluorescence spectra were recorded at 298 K with a FluoroMax4
392 spectrofluorometer (Horiba). The sample was excited at 433 nm, and FRET was detected via
393 the emission at 526 nm. The emission at 475 nm was also recorded for the FRET index
394 calculation. The FRET index (intensity at 526 nm/intensity at 475 nm) was plotted against the
395 Cl^- or L-glutamine concentration, and the titration curves were fitted to the Hill equation using
396 KaleidaGraph (Synergy Software) or ORIGIN (OriginLab).
397
398 **Isothermal titration calorimetry**
399 In order to prepare the conditions with or without Cl^-, the purified mfT1R2a/3LBD
400 heterodimer protein was dialyzed with buffers B or C, respectively. The dialyzed protein
401 solution (~50 μM) was then loaded into the sample cell in iTC200 (GE Healthcare) after the
402 removal of insoluble materials by centrifugation (10,000×*g*, 15 min, 277 K). The titration was
403 performed by injecting 2 μL of 400 μM L-glutamine at intervals of 120 s at 298 K. The
404 thermograms and the binding isotherms were analyzed with Origin software, assuming one
405 set of binding sites for fitting.
406
407 **Fluorescence-detection size-exclusion chromatography-based thermostability assay**
408 **(FSEC-TS)**
409 A T1r3-T105A mutation was introduced in the vector pAc_mfT1r3L (Yamashita *et al.*, 2017)
410 by PCR. The mutant expression vector was co-introduced with pAc_mft1r2aL (Yamashita *et*

411 *al.*, 2017) to Drosophila S2 cells to establish a stable high-expression clone cell as previously
412 described (Yamashita *et al.*, 2017). The wild-type T1r2a/T1r3LBD and mutant
413 T1r2a/T1r3-105A-LBD proteins were expressed and purified as previously described (Nango
414 *et al.*, 2016) with several modifications as listed below. After the protein binding to
415 ANTI-FLAG M2 affinity gel, the resin was washed with either buffer D (20 mM
416 HEPES-NaOH, 0.3 M NaCl, 2 mM $CaCl_2$, 5 mM L-Gln, pH 7.5) or buffer E (20 mM
417 HEPES-NaOH, 0.3 M Na gluconate, 2 mM Ca gluconate, 5 mM L-Gln, pH 7.5). Then, the
418 protein was eluted with 100 μg/mL FLAG peptide in buffer D or E.

419 The protein solutions (50 μg/mL) in buffer D or E were incubated at 4 °C, 37 °C,
420 50 °C, 70 °C, or 90 °C at 2 hours. Subsequently, the samples were loaded on an SEC-5
421 column, 500 Å, 4.6 × 300 mm (Agilent) connected to a Prominence HPLC system (Shimadzu),
422 using buffer D or E as a running buffer at a flow rate of 0.3 ml min^{-1}. The elution profiles
423 were detected with an RF-20A fluorometer (Shimadzu), using excitation and emission
424 wavelengths of 280 and 340 nm for the detection of intrinsic tryptophan fluorescence.

425 The residual ratio after incubation at each temperature was estimated using the
426 fluorescence intensity at the elution peak, which corresponded to the T1rLBD dimer, *i.e.,* the
427 peak height at ~11.6 min. The values were normalized to the intensity of the sample incubated
428 at 4 °C as 1. In order to estimate the apparent melting temperature ($T_{m\text{-}app}$) of the sample, the
429 values of residual ratio at each temperature were fitted to the Gibbs-Helmholtz equation
430 transformed as shown below (assuming that the sample protein is under equilibrium between
431 a folding and unfolding state under each condition):

$$Residual\ ratio\ = 1 - \frac{1}{1 + exp\left[-\frac{\Delta H\left(1+\frac{T}{T_{m-app}}\right) - \Delta C_P\left\{\left(T_{m-app} - \mathrm{T}\right) + Tln\left(\frac{T}{T_{m-app}}\right)\right\}}{RT}\right]}$$

432 where ΔH and ΔC_p are the enthalpy and heat capacity change of unfolding, respectively; T is
433 the temperature of the sample incubation; R is the gas constant. The fittings were performed

434 with KaleidaGraph (Synergy Software), with ΔH, ΔC_p, and $T_{m\text{-}app}$ are set as valuables.

435

436 **Single fiber recording from mouse chorda tympani (CT) nerve**

437 All animal experiments were conducted following the National Institutes of Health Guide for
438 the Care and Use of Laboratory Animals and approved by the committee for Laboratory
439 Animal Care and Use and the local ethics committee at Tokyo Dental College (Permit
440 Number: 228101) and Okayama University (Permit Number: OKU-2022897) Japan. The
441 subjects were six adult male C57BL/6JCrj mice (Charles River Japan, Tokyo, Japan) and four
442 T1r3GFP-KO mice, which were obtained by mating T1r3-GFP (Damak *et al*, 2008) and
443 T1r3-KO (Damak *et al*, 2003) mice. Mice were maintained on a 12/12-h light/dark cycle and
444 fed standard rodent chow and 8–20 weeks of age ranging in weight from 20 g to 30 g.

445 The mice were anesthetized with an injection of combination anesthetic agents
446 contained midazolam (0.8 mL/kg, Sandoz, Yamagata, Japan), medetomidine (0.75 mL/kg,
447 Nippon Zenyaku Kogyo Co., Fukushima, Japan), butorphanol tartrate (1 mL/kg, Meiji Seika
448 Pharma, Tokyo, Japan) and physiologic saline (7.45 mL/kg), and maintained at a surgical
449 level of anaesthesia, with additional injections of sodium pentobarbital (Nakarai Tesque,
450 Kyoto, Japan, 8–10 mg/kg ip every hour). Under anaesthesia, each mouse was fixed in the
451 supine position with a head holder, and the trachea cannulated. The right CT nerve was
452 dissected, free from surrounding tissues, after the removal of the pterygoid muscle and cut at
453 the point of its entry to the tympanic bulla. A single or a few nerve fibers were teased apart
454 with a pair of needles and lifted onto an Ag-AgCl electrode, and an indifferent electrode was
455 placed in nearby tissue. Their neural activities were amplified (K-1; Iyodenshikagaku,
456 Nagoya, Japan) and recorded on a computer using a PowerLab system (PowerLab/sp4; AD
457 Instruments, Bella Vista, NSW, Australia). For taste stimulation of fungiform papillae, the
458 anterior half of the tongue was enclosed in a flow chamber. Taste solutions or rinses (distilled

459 water) (~24 °C) were delivered to the tongue by gravity flow at the same flow rate (~0.1 mL
460 s^{-1}). For data analysis, we used the net average frequency for 10 sec after the stimulus onset,
461 which was obtained by subtracting the spontaneous frequency for the 10 sec duration before
462 stimulation from after stimulation. In the initial survey to identify a nerve fiber connecting to
463 T1r-expressing cells, test stimuli such as 100 mM NaCl, 10 mM HCl, 500 mM sucrose, 100
464 mM monopotassium glutamate, 20 mM quinine HCl were separately applied. If the fiber
465 responded to sucrose, we applied 10 μM–100 mM NMDG-Cl, NaCl, KCl, or either of 20 mM
466 L-glutamine or 100 mM sucrose with or without 10 mM NMDG-Cl to the tongue. The criteria
467 for the occurrence of response were the following: the number of spikes was larger than the
468 mean + two standard deviations of the spontaneous discharge for three 10 sec periods before
469 stimulation, and at least three spikes were evoked by taste stimulation (Yasumatsu *et al.*,
470 2012). In the case of T1r3GFP-KO mice, as the mice showed a significant response to 0.5 M
471 sucrose, we could identify sweet-responsive fibers (impulse frequency of 13.4 ± 1.31)
472 (Yasumatsu *et al.*, 2012). The reagents used were purchased from Wako Pure Chemical
473 Industries (Osaka, Japan; others). To block responses via T1r (Daly *et al.*, 2013; Margolskee
474 *et al.*, 2007; Ninomiya & Imoto, 1995; Ninomiya *et al.*, 1999), each tongue was treated with
475 30 μg ml^{-1} (~7 μM) gurmarin (Gur) dissolved in 5 mM phosphate buffer (pH 6.8) for 10 min,
476 similarly as described by Ninomiya & Imoto (Ninomiya & Imoto, 1995). To assure the
477 detection of responses from T1r-expressing cells, recordings from Gur-insensitive
478 sweet-responsive fibers were defined as those retaining impulse frequencies to 0.5 M sucrose
479 more than 60% after the Gur treatment (Ninomiya *et al.*, 1999) were excluded from the data.
480 The number of Gur-sensitive and Gur-insensitive fibers were six and three, respectively,
481 among 0.5 M sucrose responding fibers. The sucrose application was repeated 3–6 times
482 during the recordings. Additionally, the recovery of the suppressed responses was confirmed
483 using 15 mM β-cyclodextrin, which could remove the effect of Gur from the tongue

(Ninomiya *et al.*, 1999). All Gur-sensitive fibers recovered up to 60%–150% of responses before Gur. At the end of the experiment, animals were killed by administering an overdose of the anaesthetic. Repeated measures ANOVA and Student's paired *t*-test were used to statistically evaluate the effects of chemicals or gene deletion. The sample size was calculated according to power analysis, thereby resulting in three per group due to the effect size (d) of 6–9.3 to detect the effects of blocking or deleting T1r3.

Two-bottle preference tests

All training and testing sessions occurred during the light phase of the light/dark cycle. On the first day of training, the WT mice (adult male C57BL/6JCrj) were water deprived for 23 h and then placed in a test box with two bottles: one filled with water and the other empty. The amount of fluid intake was measured after a 5 min presentation. After 4 days of training, mice were used for test sessions if they drank water evenly on either side (nine mice). In the test sessions, they were provided with two bottles, one containing 10 mM NMDG-Cl and the other containing water, with or without Gur, for 5 min. The amount of liquid consumed was measured by weighing the bottles, and a preference score of NMDG-Cl was calculated using the following equation:

$$Preference\ score(\%) = \frac{V_{Cl}}{V_{Cl} + V_w} \times 100$$

where V_{cl} and V_w are the amount of NMDG-Cl intake and water intake, respectively.

Acknowledgments

We thank Drs. Kazuya Hasegawa, Nobuhiro Mizuno, Naohiro Matsugaki for help with X-ray data collection; Junya Nitta and Hikaru Ishida for help with protein preparation; Ryusuke Yoshida for help with the single fiber recording; Yuko Kusakabe for attempt at cell-based receptor assay in the early stage of the study; Haruo Ogawa for sharing knowledge about

ANPR; Yuzo Ninomiya for valuable discussions. We also thank the reviewers of BioPhysics Colab for their helpful comments and Enago (www.enago.jp) for the English language review. The synchrotron radiation experiments at the BL41XU, SPring-8 were performed with approvals of the Japan Synchrotron Radiation Research Institute (JASRI) (Proposal No. 2016B2534). The synchrotron radiation experiment at the BL-1A, Photon Factory was supported by the Platform for Drug Discovery, Informatics, and Structural Life Science (Proposal No. 1264). This work was financially supported by JSPS KAKENHI Grant Numbers JP17H03644, JP18H04621, JP20H03195, JP20H04778, JP21H05524 (to A.Y.) and JP20H03855, JP20K02415 (to K.Y.), Mishima Kaiun Memorial Foundation, and the Salt Science Research Foundation (Proposal No. 2039) (to A.Y.).

Competing interests

The authors declare that they have no conflict of interest.

References

Bartoshuk LM (1975) Taste mixtures: is mixture suppression related to compression? *Physiol Behav* 14: 643-649

Bartoshuk LM, McBurney DH, Pfaffmann C (1964) Taste of Sodium Chloride Solutions after Adaptation to Sodium Chloride: Implications for the "Water Taste". *Science* 143: 967-968

Bartoshuk LM, Murphy C, Cleveland CT (1978) Sweet taste of dilute NaCl: psychophysical evidence for a sweet stimulus. *Physiol Behav* 21: 609-613

Bleckmann M, Schurig M, Endres M, Samuels A, Gebauer D, Konisch N, van den Heuvel J (2019) Identifying parameters to improve the reproducibility of transient gene expression in High Five cells. *PLoS One* 14: e0217878

Cardello AV (1979) Taste quality changes as a function of salt concentration in single human

taste papillae. *Chem Senses* 4: 1-13

Chandrashekar J, Kuhn C, Oka Y, Yarmolinsky DA, Hummler E, Ryba NJ, Zuker CS (2010) The cells and peripheral representation of sodium taste in mice. *Nature* 464: 297-301

Daly K, Al-Rammahi M, Moran A, Marcello M, Ninomiya Y, Shirazi-Beechey SP (2013) Sensing of amino acids by the gut-expressed taste receptor T1R1-T1R3 stimulates CCK secretion. *Am J Physiol Gastrointest Liver Physiol* 304: G271-282

Damak S, Mosinger B, Margolskee RF (2008) Transsynaptic transport of wheat germ agglutinin expressed in a subset of type II taste cells of transgenic mice. *BMC Neurosci* 9: 96

Damak S, Rong M, Yasumatsu K, Kokrashvili Z, Varadarajan V, Zou S, Jiang P, Ninomiya Y, Margolskee RF (2003) Detection of sweet and umami taste in the absence of taste receptor T1r3. *Science* 301: 850-853

Dyr W, Wyszogrodzka E, Mierzejewski P, Bienkowski P (2014) Drinking of flavored solutions by high preferring (WHP) and low preferring (WLP) alcohol-drinking rats. *Pharmacol Rep* 66: 28-33

Ellaithy A, Gonzalez-Maeso J, Logothetis DA, Levitz J (2020) Structural and Biophysical Mechanisms of Class C G Protein-Coupled Receptor Function. *Trends Biochem Sci* 45: 1049-1064

Eriksen L, Thomsen C (1995) [3H]-L-2-amino-4-phosphonobutyrate labels a metabotropic glutamate receptor, mGluR4a. *Br J Pharmacol* 116: 3279-3287

Hattori M, Hibbs RE, Gouaux E (2012) A fluorescence-detection size-exclusion chromatography-based thermostability assay for membrane protein precrystallization screening. *Structure* 20: 1293-1299

Kabsch W (2010) Xds. *Acta Crystallogr D Biol Crystallogr* 66: 125-132

Kasahara Y, Narukawa M, Ishimaru Y, Kanda S, Umatani C, Takayama Y, Tominaga M, Oka Y, Kondo K, Kondo T *et al* (2021) TMC4 is a novel chloride channel involved in

558 high-concentration salt taste sensation. *J Physiol Sci* 71: 23

559 Keast RS, Breslin PA (2002) An overview of binary taste–taste interactions. *Food Quality and*
560 *Preference* 14: 111-124

561 Koehl A, Hu H, Feng D, Sun B, Zhang Y, Robertson MJ, Chu M, Kobilka TS, Laeremans T,
562 Steyaert J *et al* (2019) Structural insights into the activation of metabotropic glutamate
563 receptors. *Nature* 566: 79-84

564 Kuang D, Hampson DR (2006) Ion dependence of ligand binding to metabotropic glutamate
565 receptors. *Biochem Biophys Res Commun* 345: 1-6

566 Kunishima N, Shimada Y, Tsuji Y, Sato T, Yamamoto M, Kumasaka T, Nakanishi S, Jingami
567 H, Morikawa K (2000) Structural basis of glutamate recognition by a dimeric metabotropic
568 glutamate receptor. *Nature* 407: 971-977

569 Lewandowski BC, Sukumaran SK, Margolskee RF, Bachmanov AA (2016)
570 Amiloride-Insensitive Salt Taste Is Mediated by Two Populations of Type III Taste Cells with
571 Distinct Transduction Mechanisms. *J Neurosci* 36: 1942-1953

572 Li X, Staszewski L, Xu H, Durick K, Zoller M, Adler E (2002) Human receptors for sweet
573 and umami taste. *Proc Natl Acad Sci U S A* 99: 4692-4696

574 Lin S, Han S, Cai X, Tan Q, Zhou K, Wang D, Wang X, Du J, Yi C, Chu X *et al* (2021)
575 Structures of Gi-bound metabotropic glutamate receptors mGlu2 and mGlu4. *Nature* 594:
576 583-588

577 Liu H, Yi P, Zhao W, Wu Y, Acher F, Pin JP, Liu J, Rondard P (2020) Illuminating the
578 allosteric modulation of the calcium-sensing receptor. *Proc Natl Acad Sci U S A* 117:
579 21711-21722

580 Margolskee RF, Dyer J, Kokrashvili Z, Salmon KS, Ilegems E, Daly K, Maillet EL, Ninomiya
581 Y, Mosinger B, Shirazi-Beechey SP (2007) T1R3 and gustducin in gut sense sugars to
582 regulate expression of Na+-glucose cotransporter 1. *Proc Natl Acad Sci U S A* 104:

583 15075-15080

584 McCoy AJ, Grosse-Kunstleve RW, Adams PD, Winn MD, Storoni LC, Read RJ (2007) Phaser
585 crystallographic software. *J Appl Crystallogr* 40: 658-674

586 Misono KS (2000) Atrial natriuretic factor binding to its receptor is dependent on chloride
587 concentration: A possible feedback-control mechanism in renal salt regulation. *Circ Res* 86:
588 1135-1139

589 Monn JA, Prieto L, Taboada L, Hao J, Reinhard MR, Henry SS, Beadle CD, Walton L, Man T,
590 Rudyk H *et al* (2015a) Synthesis and Pharmacological Characterization of
591 C4-(Thiotriazolyl)-substituted-2-aminobicyclo[3.1.0]hexane-2,6-dicarboxylates.
592 Identification of
593 (1R,2S,4R,5R,6R)-2-Amino-4-(1H-1,2,4-triazol-3-ylsulfanyl)bicyclo[3.1.0]hexane-2,
594 6-dicarboxylic Acid (LY2812223), a Highly Potent, Functionally Selective mGlu2 Receptor
595 Agonist. *J Med Chem* 58: 7526-7548

596 Monn JA, Prieto L, Taboada L, Pedregal C, Hao J, Reinhard MR, Henry SS, Goldsmith PJ,
597 Beadle CD, Walton L *et al* (2015b) Synthesis and pharmacological characterization of
598 C4-disubstituted analogs of 1S,2S,5R,6S-2-aminobicyclo[3.1.0]hexane-2,6-dicarboxylate:
599 identification of a potent, selective metabotropic glutamate receptor agonist and determination
600 of agonist-bound human mGlu2 and mGlu3 amino terminal domain structures. *J Med Chem*
601 58: 1776-1794

602 Nango E, Akiyama S, Maki-Yonekura S, Ashikawa Y, Kusakabe Y, Krayukhina E, Maruno T,
603 Uchiyama S, Nuemket N, Yonekura K *et al* (2016) Taste substance binding elicits
604 conformational change of taste receptor T1r heterodimer extracellular domains. *Sci Rep* 6:
605 25745

606 Nelson G, Chandrashekar J, Hoon MA, Feng L, Zhao G, Ryba NJ, Zuker CS (2002) An
607 amino-acid taste receptor. *Nature* 416: 199-202

608 Nelson G, Hoon MA, Chandrashekar J, Zhang Y, Ryba NJ, Zuker CS (2001) Mammalian
609 sweet taste receptors. *Cell* 106: 381-390
610 Ninomiya Y, Imoto T (1995) Gurmarin inhibition of sweet taste responses in mice. *Am J*
611 *Physiol* 268: R1019-1025
612 Ninomiya Y, Imoto T, Sugimura T (1999) Sweet taste responses of mouse chorda tympani
613 neurons: existence of gurmarin-sensitive and -insensitive receptor components. *J*
614 *Neurophysiol* 81: 3087-3091
615 Nomura K, Nakanishi M, Ishidate F, Iwata K, Taruno A (2020) All-Electrical
616 Ca(2+)-Independent Signal Transduction Mediates Attractive Sodium Taste in Taste Buds.
617 *Neuron* 106: 816-829 e816
618 Nuemket N, Yasui N, Kusakabe Y, Nomura Y, Atsumi N, Akiyama S, Nango E, Kato Y,
619 Kaneko MK, Takagi J *et al* (2017) Structural basis for perception of diverse chemical
620 substances by T1r taste receptors. *Nat Commun* 8: 15530
621 Ogawa H, Qiu Y, Ogata CM, Misono KS (2004) Crystal structure of hormone-bound atrial
622 natriuretic peptide receptor extracellular domain: rotation mechanism for transmembrane
623 signal transduction. *J Biol Chem* 279: 28625-28631
624 Ogawa H, Qiu Y, Philo JS, Arakawa T, Ogata CM, Misono KS (2010) Reversibly bound
625 chloride in the atrial natriuretic peptide receptor hormone-binding domain: possible allosteric
626 regulation and a conserved structural motif for the chloride-binding site. *Protein Sci* 19:
627 544-557
628 Oike H, Nagai T, Furuyama A, Okada S, Aihara Y, Ishimaru Y, Marui T, Matsumoto I, Misaka
629 T, Abe K (2007) Characterization of ligands for fish taste receptors. *J Neurosci* 27: 5584-5592
630 Oka Y, Butnaru M, von Buchholtz L, Ryba NJ, Zuker CS (2013) High salt recruits aversive
631 taste pathways. *Nature* 494: 472-475
632 Roebber JK, Roper SD, Chaudhari N (2019) The Role of the Anion in Salt (NaCl) Detection

633 by Mouse Taste Buds. *J Neurosci* 39: 6224-6232

634 Roper SD (2015) The taste of table salt. *Pflugers Arch* 467: 457-463

635 Sanematsu K, Kusakabe Y, Shigemura N, Hirokawa T, Nakamura S, Imoto T, Ninomiya Y

636 (2014) Molecular mechanisms for sweet-suppressing effect of gymnemic acids. *J Biol Chem*

637 289: 25711-25720

638 Schellman JA (1975) Macromolecular Binding. *Biopolymers* 14: 999-1018

639 Stevens JC (1996) Detection of tastes in mixture with other tastes: issues of masking and

640 aging. *Chem Senses* 21: 211-221

641 Stewart RB, Russell RN, Lumeng L, Li TK, Murphy JM (1994) Consumption of sweet, salty,

642 sour, and bitter solutions by selectively bred alcohol-preferring and alcohol-nonpreferring

643 lines of rats. *Alcohol Clin Exp Res* 18: 375-381

644 Taruno A, Nomura K, Kusakizako T, Ma Z, Nureki O, Foskett JK (2021) Taste transduction

645 and channel synapses in taste buds. *Pflugers Arch* 473: 3-13

646 Tora AS, Rovira X, Cao AM, Cabaye A, Olofsson L, Malhaire F, Scholler P, Baik H, Van

647 Eeckhaut A, Smolders I *et al* (2018) Chloride ions stabilize the glutamate-induced active state

648 of the metabotropic glutamate receptor 3. *Neuropharmacology* 140: 275-286

649 Tora AS, Rovira X, Dione I, Bertrand HO, Brabet I, De Koninck Y, Doyon N, Pin JP, Acher F,

650 Goudet C (2015) Allosteric modulation of metabotropic glutamate receptors by chloride ions.

651 *FASEB J* 29: 4174-4188

652 van den Akker F, Zhang X, Miyagi M, Huo X, Misono KS, Yee VC (2000) Structure of the

653 dimerized hormone-binding domain of a guanylyl-cyclase-coupled receptor. *Nature* 406:

654 101-104

655 Yamashita A, Nango E, Ashikawa Y (2017) A large-scale expression strategy for multimeric

656 extracellular protein complexes using Drosophila S2 cells and its application to the

657 recombinant expression of heterodimeric ligand-binding domains of taste receptor. *Protein Sci*

658 26: 2291-2301

659 Yasumatsu K, Ogiwara Y, Takai S, Yoshida R, Iwatsuki K, Torii K, Margolskee RF, Ninomiya
660 Y (2012) Umami taste in mice uses multiple receptors and transduction pathways. *J Physiol*
661 590: 1155-1170

662 Ye Q, Heck GL, DeSimone JA (1991) The anion paradox in sodium taste reception: resolution
663 by voltage-clamp studies. *Science* 254: 724-726

664 Yoshida T, Yasui N, Kusakabe Y, Ito C, Akamatsu M, Yamashita A (2019) Differential
665 scanning fluorimetric analysis of the amino-acid binding to taste receptor using a model
666 receptor protein, the ligand-binding domain of fish T1r2a/T1r3. *PLoS One* 14: e0218909

667 Zhang C, Zhang T, Zou J, Miller CL, Gorkhali R, Yang JY, Schilmiller A, Wang S, Huang K,
668 Brown EM *et al* (2016) Structural basis for regulation of human calcium-sensing receptor by
669 magnesium ions and an unexpected tryptophan derivative co-agonist. *Sci Adv* 2: e1600241

670 Zhang F, Klebansky B, Fine RM, Xu H, Pronin A, Liu H, Tachdjian C, Li X (2008) Molecular
671 mechanism for the umami taste synergism. *Proc Natl Acad Sci U S A* 105: 20930-20934

672

673 **Table 1.** Properties of the Cl^--binding to T1r2a/T1r3LBD.

Cl^--binding, DSF (n = 4)		
$K_{d\text{-app}}$ (mM)	0.111 ± 0.046	
Protein thermal stability, DSF (n = 6)		
condition	+Cl^-	-Cl^-
Melting temperature (˚C)	55.2 ± 0.03	46.6 ± 0.06
Protein thermal stability, FSEC-TS		
wild type T1r2a/T1r3LBD (n = 3)		
condition	+Cl^-	-Cl^-
Melting temperature (˚C)	56.4 ± 5.1	46.0 ± 0.3
mutant T1r2a/T1r3-T105ALBD		
condition	+Cl^-	-Cl^-
Melting temperature (˚C)	42.7 ± 0.1	46.7 ± 0.7
Cl^-- binding, FRET (n = 3)		
FRET index minimum	1.00 ± 0.005	
FRET index change	0.119 ± 0.014	
EC_{50} (mM)*	1.23 ± 0.53	
L-glutamine binding, FRET (n = 3)		
condition	+Cl^-	-Cl^-
FRET index minimum	1.08 ± 0.01	0.86 ± 0.01
FRET index change	0.11	0.17
EC_{50} (μM)	3.78 ± 1.29	3.87 ± 1.76
Hill coefficient	1.20 ± 0.88	0.94 ± 0.29
L-glutamine binding, ITC		
condition	+Cl^-	-Cl^-
N (sites)	0.389 ± 0.028	0.303 ± 0.023
K_a (M^{-1})	(2.85 ± 0.65) × 10^5	(2.12 ± 0.46) × 10^5
[converted to K_d (μM)]	[3.51]	[4.72]
ΔH (kcal/mol)	-12.3 ± 1.2	–12.9 ± 1.3
ΔS (cal/mol/deg)	–16.3	-18.8

674 *Hill coefficient was fixed to 1 for fitting.

675

676 **Figure legends**

677 **Figure 1**

678 **Salt taste sensation.**

679 Approximate concentration ranges of salt taste perceptions in humans (Bartoshuk *et al.*, 1978)
680 and qualities of taste sensation with known cells and receptors responsible for their sensing
681 are summarized.

682

683 **Figure 2**

684 **Cl^--binding sites in the medaka fish taste receptor T1r2a/T1r3LBD.**

685 (**A**) Schematic drawing of the overall architecture of T1r2a/T1r3. The crystal structure (PDB
686 ID: 5X2M) (Nuemket *et al.*, 2017) is shown at the LBD region, and helices B and C in T1r3
687 are labeled. (**B**) Anomalous difference Fourier map (4.5 σ, red) of the Br^--substituted
688 T1r2a/T1r3LBD crystal. (**C**) Anomalous difference Fourier map (4.5 σ, red) of the Cl^--bound
689 T1r2a/T1r3LBD crystal derived from the diffraction data collected at the wavelength of 2.7 Å.
690 In panels B and C, the site originally identified the Cl^--binding was framed. (**D**) A close-up
691 view of the Cl^--binding site in T1r3LBD in the Cl^--bound T1r2a/T1r3LBD (PDB ID: 5X2M).
692 (**E**) Amino-acid sequence alignment of T1r proteins and the related receptors at the Cl^-
693 -binding site. The "h," "m," and "mf" prefixes to T1rs indicate human, mouse, and medaka
694 fish, respectively. The position corresponding to Thr105 in T1r3 from medaka fish is
695 highlighted. (**F**) The structures of ANPR (PDB ID: 1T34, left) (Ogawa *et al*, 2004) and
696 mGluR2 (PDB ID: 5CNI, right) (Monn *et al*, 2015a) bound with Cl^-. (**G**) Superposition of the
697 Cl^--binding site in T1r3, ANPR, and mGluR2.

698

699 **Figure 2−figure supplement 1**

700 **X-ray data collection statistics of T1r2a/T1r3LBD-Fab16A complex.**

Figure 2−figure supplement 2

The structure of the regions relating to the Cl^--binding site in medaka fish T1r2a/T1r3LBD.

(**A**) The Br^--binding site in T1r3. The anomalous difference Fourier map (4.5 σ, red) of the Br^--substituted crystal is overlayed to the Cl^--bound T1r2a/T1r3LBD structure (PDB ID: 5X2M). (**B**) The Cl^--binding site in T1r3. The anomalous difference Fourier map (4.5 σ, red) calculated from the data collected at the wavelength of 2.7 Å is overlayed. (**C**) The region in T1r2a, which corresponds to the Cl^--binding site in T1r3, in the Cl^--bound T1r2a/T1r3LBD. (**D**) The Br^--binding site in T1r2. The anomalous difference Fourier map (4.5 σ, red) is overlayed to the Cl^--bound T1r2a/T1r3LBD structure. (**E**) The Br^--binding site in T1r2. The 2.7 Å-anomalous difference Fourier map (4.5 σ, red) of the Cl^--bound T1r2a/T1r3LBD, which is the same map shown in panel B, is overlayed to the Br^--binding site in T1r2. No significant peak was observed.

Figure 2—source data 1

The anomalous difference Fourier maps shown in Figure 2B and 2C.

The structure factor files and the coordinate files used for anomalous difference Fourier calculation, and the resultant maps were included.

Figure 3

The Cl^--binding properties of T1r2a/T1r3LBD.

(**A**) Representative thermal melt curves of T1r2a/T1r3LBD in the presence of 0.003 –10 mM concentrations of Cl^- measured using DSF. (**B**) Dose-dependent T_m changes of T1r2a/T1r3LBD by addition of Cl^-. (n = 4) (**C**) Thermal melting curves of WT and the

T1r3-T105A mutant of T1r2a/T1r3LBD in the presence and absence of Cl^-, analyzed by FSEC-TS. (n = 1) (**D**) Dose-dependent FRET signal changes of the T1r2aLBD-Cerulean and T1r3LBD-Venus heterodimer by addition of Cl^-. (n = 3) (**E**) FRET index increases by adding 10 mM Cl^- or 1 mM L-glutamine to the WT or T1r3-T105A mutant T1r2aLBD-Cerulean/T1r3LBD-Venus heterodimer relative to that in the absence of any ligand in the absence of Cl^-. (n = 3) (**F**) Dose-dependent FRET signal changes of the T1r2aLBD-Cerulean and T1r3LBD-Venus heterodimer induced by the addition of L-glutamine in the presence and absence of Cl^-. (n = 3) The experiments were performed two (panels A, B, D, and E), three (C and WT), four (F and +Cl^- condition), or one (C and mutant; F and –Cl^- condition) time(s), and the results from one representative experiment are shown with numbers of technical replicates. Data points represent mean and s.e.m.

Figure 3–figure supplement 1

The properties of T1r2a/T1r3LBD in the presence and absence of Cl^-.

(**A**) Binding analysis of gluconate by DSF. 0.1, 1, and 10 mM of L-glutamine, as a representative ligand, and sodium gluconate was added to T1r2a/T1r3LBD in 20 mM HEPES-NaOH, 300 mM NaCl, pH 7.5. The mean increases of T_m (ΔT_m) from that in the absence of a ligand (54.1 ˚C, measured on the same sample, n = 2) are plotted. Error bars are in s.e.m. (n = 4). (**B**) Representative thermal melt curves of T1r2a/T1r3LBD in the presence or absence of Cl^-, measured by DSF in the same condition in Figure 3C, and the panels C, D in this figure. (**C**, **D**) The L-glutamine-binding to T1r2a/T1r3LBD was measured by isothermal titration calorimetry. The upper and lower panels show the raw data and integrated heat signals upon L-glutamine injection to T1r2a/T1r3LBD in the presence (C) and absence (D) of Cl^-. The binding isotherms were fitted assuming 1 ligand: 1 heterodimer binding. The experiments were performed one (panel A), two (B) four (C), or five (D) time(s), and the

751 results from one representative experiment are shown with numbers of technical replicates.

752

753 **Figure 3—source data 1**

754 **Excel file with numerical data used for Figure 3.**

755

756 **Figure 4**

757 **Electrophysiological and behavioral analyses of the T1r-mediated Cl^- responses in**

758 **mouse.**

759 (**A**–**D**) Results of single fiber recordings from the mouse chorda tympani nerve. (**A**)

760 Representative recordings of single fibers that connect to T1r-expressing taste cells. The

761 stimuli were 10 mM NMDG-Cl, 100 mM sucrose, 100 mM sucrose + 10 mM NMDG-Cl, 20

762 mM L-glutamine, or 20 mM L-glutamine + 10 mM NMDG-Cl. Lines indicate the application

763 of stimuli to the tongue. All the responses were suppressed by lingual treatment with a T1r

764 blocker, Gur (right). (**B**) Impulse frequencies in response to the concentration series of

765 NMDG-Cl, NaCl, or KCl before and after Gur treatment in WT mice. Responses to

766 NMDG-gluconate are also shown. The mean number of net impulses per 10 s (mean

767 response) ± s.e.m. in Gur-sensitive fibers (n = 5–6 from six mice). (**C**) Impulse frequencies in

768 response to the concentration series of NMDG-Cl before and after Gur treatment were

769 measured in T1r3-KO mice (n = 4–5 from three mice). Responses to NMDG-gluconate are

770 also shown. (**D**) Impulse frequencies to 20 mM L-glutamine or 100 mM sucrose in the

771 absence or presence of 10-mM NMDG-Cl before and after Gur treatment. Responses to 20

772 mM L-glutamine or 100 mM sucrose by T1r3-KO mouse are also shown. Values are mean ±

773 s.e.m. (n = 3–5 from three mice each). *, **: paired t-test; $P < 0.05$ (*) and < 0.01 (**). (**E**)

774 Amount of fluid intake for water and 10-mM NMDG-Cl in the two-bottle preference tests.

775 Values are mean ± s.e.m. (n = nine mice) (**F**) NMDG-Cl intake shown in (E) normalized to

776 water intake (preference score) in the two-bottle preference tests. A score > 50% indicates that
777 the taste solution was preferred over water.
778
779 **Figure 4—source data 1**
780 **Excel file with numerical data used for Figure 4.**
781
782 **List of Figure supplements and source data**
783 Figure 2—figure supplement 1
784 Figure 2—figure supplement 2
785 Figure 2—source data 1
786 Figure 3—figure supplement 1
787 Figure 3—source data 1
788 Figure 4—source data 1
789

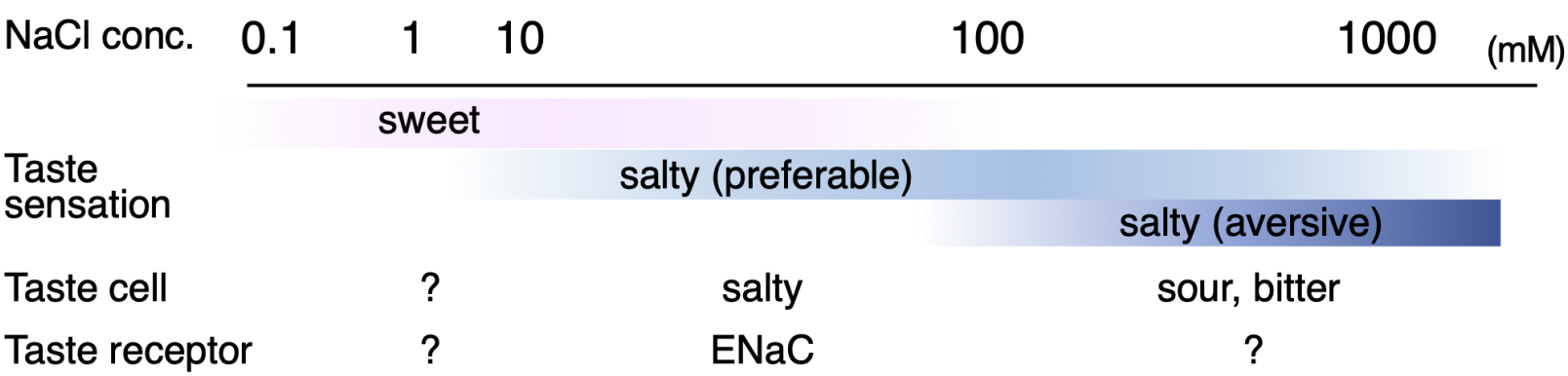

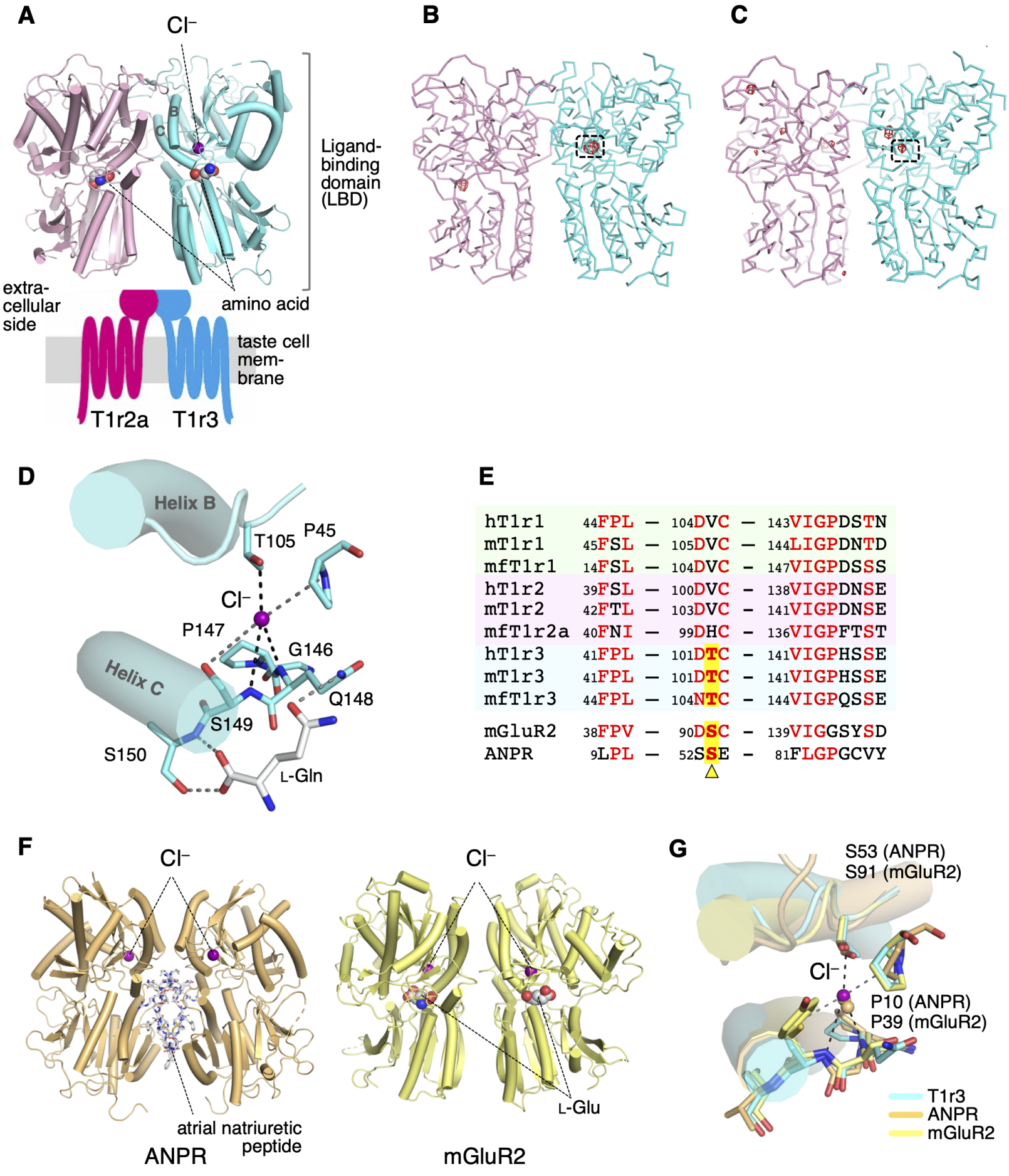

X-ray data collection statistics of T1r2a/T1r3LBD-Fab16A complex.

	Br^--bound	**Cl^--bound**
Beamline	SPring-8 BL41XU	Photon Factory BL-1A
Detector	PILATUS6M	EIGER X4M
Wavelength (Å)	0.9194	2.7
Space group	$P2_12_12_1$	$P2_12_12_1$
Cell dimensions		
a (Å)	102.8	102.8
b (Å)	121.6	120.8
c (Å)	129.9	129.1
Resolution (Å)	50-3.41 (3.43-3.41)	49.8-3.32 (3.33-3.32)
R_{sym} (%)*	0.094 (0.808)	0.089 (0.865)
$I/\sigma(I)$*	16.4 (2.3)	15.1 (2.45)
Completeness (%)*	99.8 (99.2)	99.6 (97.8)
Redundancy*	7.0 (7.0)	6.9 (6.8)

*Values in parentheses refer to data in the highest resolution shells.